Thin Solid Films 571 (2014) 206–211

Contents lists available at ScienceDirect

Thin Solid Films

journal homepage: www.elsevier.com/locate/tsf

Hydrogen, oxygen and hydroxyl on porous silicon surface: A joint density-functional perturbation theory and infrared spectroscopy approach

Pedro Alfaro, Alessio Palavicini, Chumin Wang *

Instituto de Investigaciones en Materiales, Universidad Nacional Autónoma de México, Apartado Postal 70-360, C.P. 04510, D.F. Mexico, Mexico

ARTICLE INFO

Article history:
Received 29 April 2014
Received in revised form 17 October 2014
Accepted 24 October 2014
Available online 30 October 2014

Keywords:
Porous silicon
Oxygen adsorption
Infrared spectrum
Ab-initio calculations

ABSTRACT

Based on the density functional perturbation theory (DFPT), infrared absorption spectra of porous silicon are calculated by using an ordered pore model, in which columns of silicon atoms are removed along the [001] direction and dangling bonds are initially saturated with hydrogen atoms. When these atoms on the pore surface are gradually replaced by oxygen ones, the ab-initio infrared absorption spectra reveal oxygen, hydroxyl, and coupled hydrogen–oxygen vibrational modes. In a parallel way, freestanding porous silicon samples were prepared by using electrochemical etching and they were further thermally oxidized in a dry oxygen ambient. Fourier transform infrared spectroscopy was used to investigate the surface modifications caused by oxygen adsorption. In particular, the predicted hydroxyl and oxygen bound to the silicon pore surface are confirmed. Finally, a global analysis of measured transmittance spectra has been performed by means of a combined DFPT and thin-film optics approach.

1. Introduction

Porous silicon (PSi) is a nanostructured material with interesting properties, such as a huge surface area useful for sensor applications, a tunable refractive index and an efficient photo- and electroluminescence for photonic devices [1], in addition to its compatibility with the current microelectronics based on silicon since it is the second most abundant element in Earth's crust. The extensive surface area of PSi makes it chemically unstable and prone to oxidation in the atmosphere. For crystalline silicon (*c*-Si), the oxidation process has been widely studied, since SiO_2 is one of the best electrical insulators [2]. Such oxidation begins with the adsorption of oxygen atoms on the *c*-Si surface by forming Si – OH and Si – O – Si bonds [3]. In order to identify the nature of oxygen bonds on the nanostructured PSi surface under different oxidation conditions, we develop a microscopic model of PSi oxidation and calculate its effects on the infrared (IR) absorption spectra. The theoretical results are further compared with experimental measurements.

From a theoretical viewpoint, microscopic modeling of porous structures is a difficult endeavor. There are essentially two options: semi-empirical, such as empirical pseudopotentials and tight-binding based on atomic orbitals or Wannier's functions, and ab-initio approaches, through density functional theory with GW correction or quantum Monte Carlo calculations [4]. The former has the advantage of being simple and able to address complex porous structures. However, it is not suitable for studying oxidation since the presence of oxygen atoms distorts the structure and requires a questionable rescaling of the involved microscopic parameters, in contrast to the hydrogen passivation case. On the other hand, the ab-initio calculations are more accurate but allow the treatment of simple porous structures only. In this article we choose the second option, *i.e.*, modeling [5] the PSi structure by using the supercell technique within the density functional theory (DFT), through a double self-consistent procedure: one for the electronic density distribution and another for the geometrical optimization to determine the atomic positions of minimal energy. In addition, the calculation of IR absorption spectra requires the determination of atomic vibrational modes. The density functional perturbation theory (DFPT) [6] provides a natural way of inserting the dynamical-matrix calculation into the mentioned self-consistent procedures. On the other hand, we measure the IR transmittance spectra of oxidized free-standing PSi layers and compare them with the calculated spectra.

2. Ab-initio modeling

PSi possesses a complex morphology and its theoretical modeling has been carried out by using Si clusters [7], Si nanowires [8] and periodic porous structure [9]. In general, oxidation of the c-Si surface produces Si – O – Si and Si – OH bonds [10], which can be detected by means of IR spectroscopy. In order to analyze the IR modes of these bonds in the three mentioned structures, we first performed a comparative study of the IR absorption peaks employing supercells of $16.3 \times 16.3 \times 16.3$ Å^3 for the cluster case and $16.3 \times 16.3 \times 5.43$ Å^3 for nanowire and porous

* Corresponding author. Tel.: +52 55 56224634; fax: +52 55 56161251.
E-mail address: chumin@unam.mx (C. Wang).

http://dx.doi.org/10.1016/j.tsf.2014.10.084
0040-6090/

structures, where periodic boundary conditions are considered in the *x*, *y* and *z* directions. The supercell of the porous structure was built by joining on the *x*–*y* plane nine unit cells of eight Si atoms each.

The calculations were carried out within DFT through the generalized gradient approximation with the Perdew–Burke–Ernzerhof functional and norm-conserving pseudopotentials. A full geometry optimization was performed using the Broyden–Fletcher–Goldfarb–Shanno minimization algorithm for the three structures, where a cutoff energy of 830 eV was used. The Monkhorst–Pack mesh of $1 \times 1 \times 1$ was used for the case of molecule and $1 \times 1 \times 3$ for the nanowire and porous structures. All the ab-initio calculations in this article were performed with the CASTEP codes developed at Cambridge University within Accelrys Materials Studio 7.0 [11] on ultrafine precision, where the convergence criteria are 5×10^{-6} eV/atom for the energy, 0.01 eV/Å for the force and 0.02 GPa for the stress. All the structure sketches in this article are obtained after the geometry optimization. Fig. 1(a) shows the smallest cluster structure to include Si – O – Si and Si – OH bonds. In the nanowire case, we started with a periodic silicon wire lying along the [001] direction with a 3×3 atoms square cross-section. Then, Si – O – Si and Si – OH bonds were added to the wire sidewall at opposite corners, while the surface dangling bonds were saturated with hydrogen, as illustrated in Fig. 1(b). On the other hand, the porous structure was constructed by digging empty columns along the [001] direction in an otherwise c-Si structure, *i.e.*, removing 40 Si atoms from a 72 atom supercell. Fig. 1(c) is a [001] view of the resulting structure. Once the geometrical optimization was performed, we further calculate the structural vibrational modes and the IR absorption spectra by means of the DFPT [6]. The obtained IR spectra are shown in Figs. 1(a′) for cluster, 1(b′) for nanowire and 1(c′) for porous structure.

Based on experimental IR absorption bands of Si – O – Si in siloxanes [12], Si – H in silanes [13], and Si – OH in silanols [12], Table 1 summarizes the corresponding calculated absorption peaks and bands obtained from Fig. 1(a′–c′), where the peak with the highest wavenumber within the band near 1000 cm^{-1} is associated to the Si – O – Si vibrational modes. Observe a systematic shift towards lower wavenumbers of the peaks corresponding to the nanowire and porous structures in comparison with the molecule absorption peaks. This fact could be related to the higher mass involved in these vibrational modes for these two structures.

Now we focus on the porous structure model to analyze the oxidation process in PSi by starting from a fully hydrogenated surface and gradually substituting hydrogen atoms by oxygen. Fig. 2(a)–(i) respectively illustrate the progressive addition of oxygen atoms from zero to eight, modeling different oxidation stages by forming Si – O – Si bonds in an originally 32 Si-atom supercell. The corresponding calculated IR transmittance spectra are shown in Fig. 2(a′–i′), obtained from the same calculation procedure used in Fig. 1.

Observe the absorption band at 2070–2200 cm^{-1}, which is related to the Si – H vibrational modes, and that its amplitude diminishes as the hydrogen content decreases. The 917–938 cm^{-1} band is associated to coupled hydrogen–oxygen vibrational modes on the PSi surface. In fact, this band disappears when the surface is fully passivated by oxygen atoms.

Another radical found in the oxidation process of c-Si is hydroxyl (OH) [12]. For its analysis, larger supercells are needed since the pores contained in a 32-Si-atom supercell, as in Fig. 2, are not big enough to fit several of these radicals without a significant interaction between them. Thus, we resort to a 72-Si-atom supercell, as shown in Fig. 1(c), to study the effects of OH on the IR response. Fig. 4 illustrates the studied structures passivated by (a′) hydrogen and OH, as well as (b′) hydrogen, OH and oxygen. The corresponding calculated IR transmittance spectra are shown in Fig. 4(a) and (b), respectively.

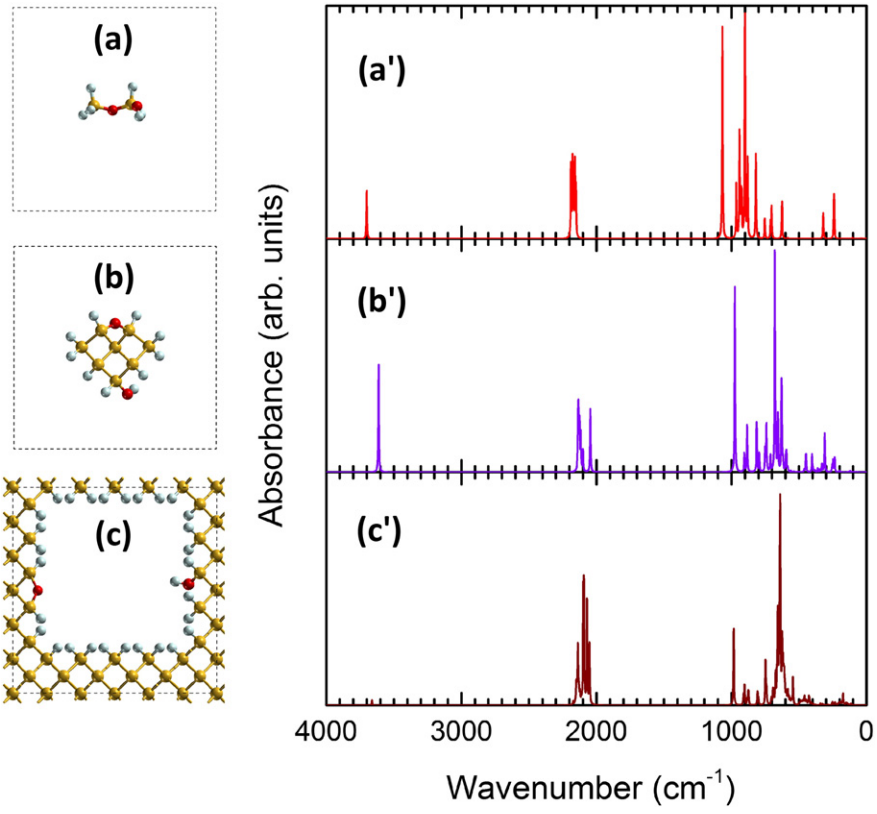

Fig. 1. Sketches of Si (yellow spheres), H (gray spheres) and O (red spheres) in (a) $H_6Si_2O_2$ molecule, (b) nanowire and (c) porous structure, where the dashed lines indicate the supercell boundaries of $16.3 \times 16.3 \times 16.3$ Å^3 for (a) and $16.3 \times 16.3 \times 5.43$ Å^3 for (b) and (c). The calculated IR absorbance spectra (a′–c′) are shown for (a–c), respectively.

Table 1
Main IR absorption peaks of $H_6Si_2O_2$ molecule, Si nanowire and porous structure.

Functional group	Molecule	Nanowire	Porous structure	Experiment
Si – O – Si	1067 cm^{-1}	975 cm^{-1}	984 cm^{-1}	1000–1100 cm^{-1} [12]
Si – H	2152–2188 cm^{-1}	2045–2136 cm^{-1}	2051–2173 cm^{-1}	2100–2250 cm^{-1} [13]
Si – OH	3701 cm^{-1}	3613 cm^{-1}	3662 cm^{-1}	3200–3700 cm^{-1} [12]

3. Experimental results

In order to confirm the ab-initio results, we further fabricate PSi samples by means of an anodic electrochemical dissolution of boron-doped *p*-type (100)-oriented *c*-Si wafers with an electrical resistivity of 0.01–0.03 Ω-cm in an electrolyte consisting of a mixture of HF (49%) and ethanol (99.9%) with a volume ratio of 1:2. A gold film of 30 nm was deposited on the backside of *c*-Si wafers to ensure electrical contact during the anodization. In the course of etching process, a dc electrical current of 75 mA was applied for 900 s between the platinum electrode and the wafer backside contact. To remove the PSi layer from the wafer, an additional dc current of 1100 mA for 5 seconds was further applied, producing a freestanding PSi film with a thickness of 28.6 μm measured by scanning electron microscopy (SEM). A mechanical pump was used to recycle the electrolyte in order to remove air bubbles generated by the electrochemical reaction. The etched area was approximately 2.6 cm^2. After etching, the samples were rinsed with ethanol and dried in air at room temperature. The freestanding PSi samples were further thermally oxidized at temperatures of 200, 400, and 600 °C in a dry oxygen atmosphere for 20 min, using a Carbolite MTF10 horizontal electric tube furnace. The nanoscale morphology of the samples was examined by SEM using a JEOL JSM-7600F. Fig. 3(a) shows a SEM image of the surface (top) view, while Fig. 3(b) and (b′) are two cross-section (side) views of a PSi layer fabricated by using the same etching parameters as the freestanding samples. The electron acceleration voltage used was 2.5 kV for Fig. 3(a)–(b) and 10 kV for Fig. 3(b′). The top-view image was analyzed with the aid of ImageJ software in order to obtain the PSi layer porosity, which was calculated as the ratio of pore to total area. The pores were determined by the black spots resulting from a conversion of grayscale to black-and-white images, whose threshold was obtained through the Rényi Entropy method that maximizes the information between the object and the background [14]. The resulting threshold of 123 from a 0–255 grayscale gives rise to a porosity of 48.2%, which is close to the porosity measured from gravimetric and nitrogen adsorption techniques [15]. Fig. 3(a′), obtained from 3(a), presents the pore-diameter distribution in logarithmic scale with a bin size of 0.74 nm. Notice that there are two distinctive regions spanning (0 − 3.7nm) and (3.7 − 45.0 nm). The former, composed of the first five bars, has a higher frequency and exponential decay since it corresponds to small black spots made of 1 to 5 pixels, being 0.625 nm the pixel length. The latter possesses a qualitatively different behavior that can be well described by a Weibull distribution [16]. On the other hand, Fig. 3(b) reveals a branched structure of pores with preferential growth in the [100] crystalline direction, while Fig. 3(b′) illustrates the PSi layer thickness of 28.6 μm with a narrowing close to the border of the anodization zone due to a non-uniform distribution of the applied electrical field towards the border.

The refractive index of PSi layers can be calculated through the Bruggeman effective medium theory, which considers a system made up of two spherical inclusions, *i.e.*, air and c-Si in a matrix with effective dielectric constant $\bar{\varepsilon}$ determined by [17]

$$p\frac{\varepsilon_{\text{Air}}-\bar{\varepsilon}}{\varepsilon_{\text{Air}}+2\bar{\varepsilon}}+(1-p)\frac{\varepsilon_{\text{c-Si}}-\bar{\varepsilon}}{\varepsilon_{\text{c-Si}}+2\bar{\varepsilon}}=0 \quad (1)$$

where p is the sample porosity, $\varepsilon_{\text{Air}} = 1$ and $\varepsilon_{\text{c - Si}} = 11.63$ are respectively the dielectric constants of air and *c*-Si for a photon energy of 0.25 eV [18]. The refractive index of oxidized PSi can also be modeled

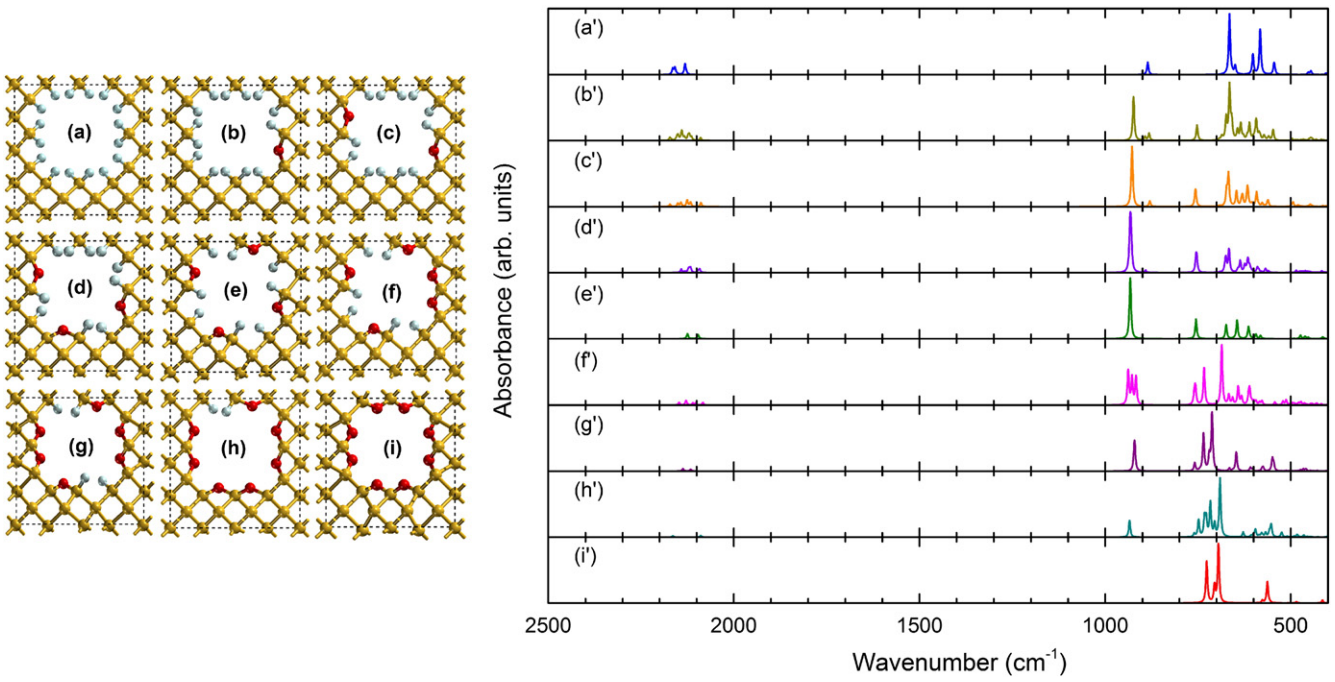

Fig. 2. Schematic representation of geometrically-optimized 10.8 × 10.8 × 5.4 $Å^3$ supercells made of 20 silicon (yellow spheres), (a) 16 hydrogen (gray spheres) and zero oxygen (red spheres) up to (i) zero hydrogen and 8 oxygen atoms, in each case substituting two hydrogen atoms by an oxygen one. Figs. 2(a′)–2(i′) show calculated IR absorbance spectra of the corresponding supercells 2(a)–2(i).

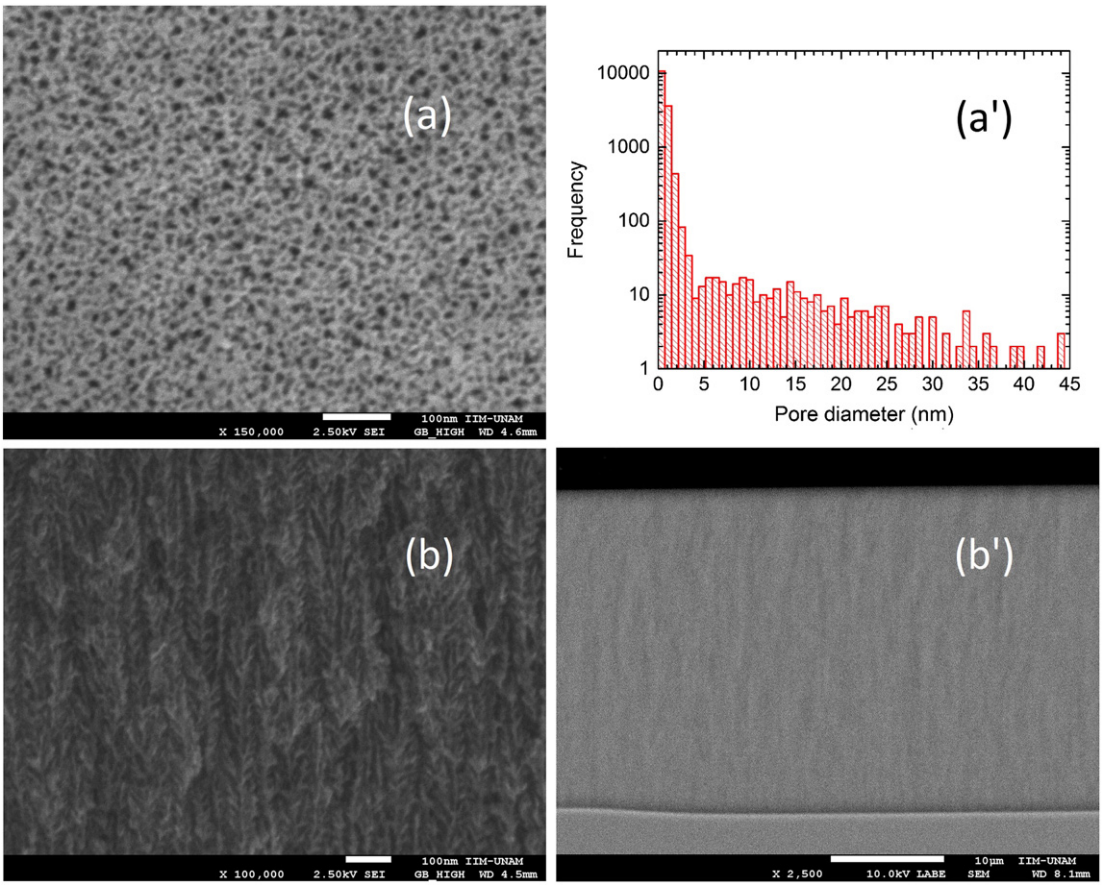

Fig. 3. SEM images of (a) top, (b) and (b′) side views of a fresh PSi layer, where the scale bars indicate (a) 100 nm, (b) 100 nm, and (b′) 10 μm. Fig. 3(a′) shows the pore diameter distribution obtained from 3(a).

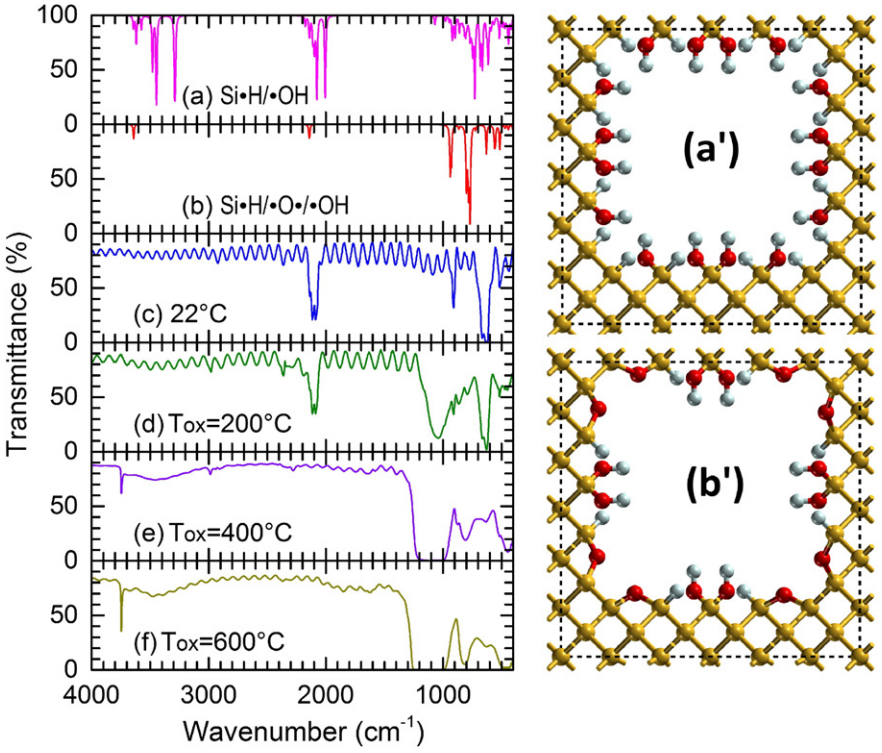

Fig. 4. (a–b) Calculated IR transmittance spectra of pore structures passivated by (a′) hydrogen plus OH and (b′) hydrogen, OH plus oxygen. The experimental IR spectra of PSi free standing samples are shown in Fig. 4(c) for fresh, thermally oxidized 4(d) at 200 °C, 4(e) at 400 °C and (f) at 600 °C for 20 min.

through a three-part mix of air/silicon/silica, whose relative volumes can be determined by ellipsometric measurements [19]. The porosity (p) is also measured through a gravimetric method given by [20]

$$p = \frac{\Delta m}{\rho_{c\text{-}Si} A d}, \tag{2}$$

where $\rho_{c\text{-}Si} = 2.329\ \mathrm{g/cm^3}$ is the density of c-Si, $d = 0.029$ cm and $A = 2.6\ \mathrm{cm^2}$ are respectively the thickness and area of the PSi layer, and $\Delta m = m_i - m_f = 0.00832$ g is the mass difference of the sample before (m_i) and after (m_f) anodization measured on a Mettler Toledo XP105DR analytic balance. The resulting porosity is approximately 48 %. Therefore, Eq. (1) yields an effective dielectric constant of $\bar{\varepsilon} = 4.71$ and a refractive index of $n_{PSi} = \sqrt{\bar{\varepsilon}} = 2.17$.

In Fig. 4 the measured IR transmittance spectra of freestanding samples obtained using an Fourier Transform Infrared Shimadzu IRAffinity spectrophotometer are shown for (c) as-prepared, thermally oxidized (d) at 200 °C, (e) at 400 °C and (f) at 600 °C for 20 min. Observe the remarkable oscillation present in Fig. 4(c) and 4(d) with average periods of 79.5 and 100 $\mathrm{cm^{-1}}$, respectively. This oscillation is originated by multiple light reflections within the PSi layer [21]. In general, the light transmittance (T) for normal incidence of a single PSi layer immersed in air is given by [22]

$$T = |t|^2 = \left| \frac{\left(1-\xi^2\right)e^{-i\phi}}{1-\xi^2 e^{-2i\phi}} \right|^2 = \frac{\left(1-\xi^2\right)^2}{1-\xi^2 2\cos(2\phi)+\xi^4}, \tag{3}$$

where $\xi = \frac{n_{PSi}-1}{n_{PSi}+1}$ and $\phi = \frac{2\pi n_{PSi} d}{\lambda}$, being λ the wavelength of incident light. The period (τ) of this oscillation derived from Eq. (3) is $\tau = 1/(2n_{PSi}d) \approx 80.56\ cm^{-1}$, which is close to the average oscillation period in the transmittance spectrum of Fig. 4(c). For the oxidized samples, a larger oscillation period of 100 $\mathrm{cm^{-1}}$ is observed, which leads to a smaller refractive index and this in turn to the smaller oscillation amplitudes appearing in Fig. 4(d–f). This calculation assumes that the PSi layer is a perfect dielectric with zero absorbance.

On the other hand, the IR absorbance can be addressed by ab-initio quantum calculations, as presented in Fig. 4(a) and (b) for 72-Si-atom supercells. Notice the absorption band located at 2000–2200 $\mathrm{cm^{-1}}$ in Fig. 4(c) and (d) for fresh and 200 °C oxidized samples, which is related to the Si–H vibrational modes, and it essentially disappears in Fig. 4(e) and (f) for the 400 °C and 600 °C oxidized samples. This behavior is consistent with the ab-initio results of Fig. 4(b). In the 3000–3700 $\mathrm{cm^{-1}}$ region, there is a remarkable absorption band in the 400 and 600 °C-oxidized spectra shown in Fig. 4(e) and (f), which indicates an abundance of OH radicals as in Fig. 4(a). At the end of this band there is a sharp peak located at 3746 $\mathrm{cm^{-1}}$ with a full width at half maximum of 10 $\mathrm{cm^{-1}}$, which is associated to the Si–OH stretching vibrational mode [23]. Finally, observe the rapid growth from Fig. 4(d) to (f) of the Si–O–Si band at 900–1200 $\mathrm{cm^{-1}}$.

4. Conclusions

This article reports an ab-initio study of the oxidation in PSi by using the DFPT and an ordered pore model. This model has the advantage of emphasizing both the quantum confinement and the interconection throughout the porous structure, which allows the calculation of coherent vibrational modes in inelastic light scattering [24] as well as transport properties. The IR absorbance spectrum obtained through this pore model shows comparable results from those of cluster and nanowire approaches, whose difference arises from the inertial mass involved. A progressive subtitution of hydrogen with oxygen atoms on the pore surface reveals the vanishing of the band located at 2070–2200 $\mathrm{cm^{-1}}$, as well as the appearance and further fading of a narrow band at 917–938 $\mathrm{cm^{-1}}$. In a parallel way, we have produced thermally-oxidized PSi freestanding samples and measured their porosity through image analysis and gravimetric methods obtaining consistent results. This consistance does not necessarily occur for high porosity samples since the gravimetric method frequently overestimates the porosity. We further measure their IR transmittance spectra, observing a good agreement with the DFPT ab-initio results. Although the DFT is designed to treat only the ground state, this study shows the potential of DFPT to analyze properties of low-energy excited states. On the other hand, the oscillating behavior observed in the transmittance spectrum of fresh PSi sample is accurately described by an effective-medium electromagnetic model without fitting parameters, in which the PSi layer is treated as a perfect dielectric. The amplitude of this oscillation diminishes as the oxidation temperature increases, which could be due to a lower refractive index of the oxidized PSi layer caused by oxygen diffusion into the bulk structure as suggested by X-ray analysis [25]. Finally, this study confirms hydrogen and hydroxyl species on the fresh and thermally oxidized pore surface, respectively. In the case of oxygen, we observe a full absorption band at 1000–1200 $\mathrm{cm^{-1}}$ [26,27], which is difficult to decompose and compare with the individual vibrational modes predicted by the ab-initio calculations. Moreover, this study tests the predictive capability of DFPT ab-initio studies beyond ground-state properties, and the possibility of combining the classical optics, Bruggeman effective medium theory and quantum ab-initio approaches to study IR transmittance spectra of PSi layers.

Acknowledgments

We would like to thank Rodolfo Cisneros for useful discussions, Omar Novelo and Yolanda Flores for their technical assistance. This work has been partially supported by CONACyT-131596 and UNAM-IN113714. Computations have been performed at Miztli of DGTIC, UNAM. One of the authors (P.A.) acknowledges the Program of Post-Doctoral Scholarships in the UNAM (2012–2013) and the support from the Consejo Nacional de Ciencia y Tecnología (2014).

References

[1] G. Korotcenkov, B.K. Cho, Silicon porosification: state of the art, Crit. Rev. Solid State Mater. Sci. 35 (2010) 153, http://dx.doi.org/10.1080/10408436.2010.495446.
[2] J.F. Shackelford, W. Alexander (Eds.), CRC Materials Science and Engineering Handbook, third ed.CRC Press, Boca Raton, 2001, p. 986.
[3] T. Engel, The interaction of molecular and atomic oxygen with Si(100)and Si(111), Surf. Sci. Rep. 18 (1993) 93, http://dx.doi.org/10.1016/0167-5729(93)90016-I.
[4] J. Tagüeña-Martínez, C. Wang, Electronic band structure in porous silicon, to be published, in: L.T. Canham (Ed.), Handbook of Porous Silicon, Springer, 2014.
[5] Y. Bonder, C. Wang, A first-principles model of birefringent porous silicon, J. Appl. Phys. 100 (2006) 044319, http://dx.doi.org/10.1063/1.2335669.
[6] S. Baroni, S. de Gironcoli, A. Dal Corso, P. Giannozzi, Phonons and related crystal properties from density-functional perturbation theory, Rev. Mod. Phys. 73 (2001) 515, http://dx.doi.org/10.1103/RevModPhys.73.515.
[7] C. Delerue, M. Lannoo, G. Allan, E. Martin, Theoretical descriptions of porous silicon, Thin Solid Films 255 (1995) 27, http://dx.doi.org/10.1103/PhysRevB.48.11024.
[8] P.V. Avramov, A.A. Kuzubov, A.S. Fedorov, P.B. Sorokin, F.N. Tomilin, Y. Maeda, Density-functional theory study of the electronic structure of thin Si/SiO_2 quantum nanodots and nanowires, Phys. Rev. B 75 (2007) 205427, http://dx.doi.org/10.1103/PhysRevB.75.205427.
[9] M. Cruz, C. Wang, M.R. Beltrán, J. Tagüeña-Martínez, Morphological effects on the electronic band structure of porous silicon, Phys. Rev. B 53 (1996) 3827, http://dx.doi.org/10.1103/PhysRevB.53.3827.
[10] Y. Ogata, H. Niki, T. Sakka, M. Iwasaki, Oxidation of porous silicon under water vapor environment, J. Electrochem. Soc. 142 (1995) 1595, http://dx.doi.org/10.1149/1.2048619.
[11] M.D. Segall, P.J.D. Lindan, M.J. Probert, C.J. Pickcard, P.J. Hasnip, S.J. Clark, M.C. Payne, First-principles simulation: ideas, illustrations and the CASTEP code, J. Phys. Condens. Matter 14 (2002) 2717, http://dx.doi.org/10.1088/0953-8984/14/11/301.
[12] E.D. Lipp, A.L. Smith, Infrared, raman, near-infrared, and ultraviolet spectroscopy, in: A.L. Smith (Ed.), The Analytical Chemistry of Silicones, John Wiley and Sons, New York, 1991, p. 305.
[13] S.D. Gokhale, W.L. Jolly, Some properties of n- and isotetrasilane, Inorg. Chem. 3 (1964) 946, http://dx.doi.org/10.1021/ic50017a004.
[14] J.N. Kapur, P.K. Sahoo, A.C.K. Wong, A new method for gray-level picture thresholding using the entropy of the histogram, Comput. Vision Graph. Image Process. 29 (1985) 273, http://dx.doi.org/10.1016/0734-189X(85)90125-2.

[15] R. Herino, G. Bomchil, K. Barla, C. Bertrand, J.L. Ginoux, Porosity and pore size distributions of porous silicon layers, J. Electrochem. Soc. 134 (1987) 1994, http://dx.doi.org/10.1149/1.2100805.
[16] N. Narayanan, M.S. Sumanasooriya, O. Deo, Characterizing pore volume, sizes, and connectivity in pervious concretes for permeability prediction, Mater. Charact. 61 (2010) 802, http://dx.doi.org/10.1016/j.matchar.2010.05.004.
[17] D.A.G. Bruggeman, Berechnung verschiedener physikalischer Konstanten von heterogenen Substanzen, Ann. Phys. (Leipzig) 24 (1935) 636, http://dx.doi.org/10.1002/andp.19354160705.
[18] D.E. Aspnes, Optical properties, in: R. Hull (Ed.), Properties of Crystalline Silicon, INSPEC, London, 1999, p. 677.
[19] R. Cisneros, C. Ramírez, C. Wang, Ellipsometry and ab initio approaches to the refractive index of porous silicon, J. Phys. Condens. Matter 19 (2007) 395010, http://dx.doi.org/10.1088/0953-8984/19/39/395010.
[20] V. Lehman, Electrochemistry of Silicon, Wiley-VCH, Weinheim, 2002. 97.
[21] A. Palavicini, C. Wang, Infrared transmission in porous silicon multilayers, Opt. Photonics J. 3 (2013) 20, http://dx.doi.org/10.4236/opj.2013.32A003.
[22] P. Yeh, Optical Waves in Layered Media, John Wiley, New Jersey, 2005. 83.
[23] D.B. Mawhinney, J.A. Glass Jr., J.P. Yates Jr., FTIR study of the oxidation of porous silicon, J. Phys. Chem. B 101 (1997) 1202, http://dx.doi.org/10.1021/jp963322r.
[24] P. Alfaro, R. Cisneros, M. Bizarro, M. Cruz-Irisson, C. Wang, Raman scattering by confined optical phonons in Si and Ge nanostructures, Nanoscale 3 (2011) 1246, http://dx.doi.org/10.1039/C0NR00623H.
[25] R. Cisneros, H. Pfeiffer, C. Wang, Oxygen absorption in free-standing porous silicon: a structural, optical and kinetic analysis, Nanoscale Res. Lett. 5 (2010) 686, http://dx.doi.org/10.1007/s11671-010-9532-2.
[26] Y. Kanemitsu, T. Futagi, T. Matsumoto, H. Mimura, Origin of the blue and red photoluminescence from oxidized porous silicon, Phys. Rev. B 49 (1994) 14732, http://dx.doi.org/10.1103/PhysRevB.49.14732.
[27] J.Y. Park, J.H. Lee, Characterization of 10 μm thick porous silicon dioxide obtained by complex oxidation process for RF application, Mater. Chem. Phys. 82 (2003) 134, http://dx.doi.org/10.1016/S0254-0584(03)00187-1.